# Microwave-Assisted Hydrothermal Synthesis of SrTiO$_3$:Rh for Photocatalytic Z-scheme Overall Water Splitting

**Hsin-yu Lin * and Lyu-Ting Cian**

Department of Materials Science and Engineering, National Dong Hwa University, Hualien 97401, Taiwan; a856865@gmail.com

* Correspondence: hsinyu@gms.ndhu.edu.tw; Tel.: +886-3-890-3231

check for updates

**Abstract:** Developing a photocatalyst system for solar energy conversion to electric energy or chemical energy is a topic of great interest for fundamental and practical importance. In this study, hydrogen production by a new Z-scheme photocatalysis water-splitting system was examined over Rh-doped SrTiO$_3$ (denoted as Rh:SrTiO$_3$) with Ru nanoparticle as cocatalyst for H$_2$ evolution and BiVO$_4$ photocatalyst for O$_2$ evolution under visible light irradiation, where Co(bpy)$_3^{2+/3+}$ was used as electron mediator. The catalysts were characterized by powder X-ray diffraction (XRD), scanning electron microscope (SEM), transmission electron microscopy (TEM), and Ultraviolet–visible spectroscopy. We present a fast and efficient method to synthesize Rh-doped SrTiO$_3$ photocatalyst via microwave-assisted hydrothermal method. Our results showed a significant effect of Ti precursor on morphology of Rh:SrTiO$_3$ prepared by microwave-assisted hydrothermal synthesis. The Ru/Rh:SrTiO$_3$ prepared by TiCl$_4$ precursor showed a nanoporous structure and high photocatalytic activity. The combination of Ru/Rh:SrTiO$_3$ with BiVO$_4$ achieves a high H$_2$ evolution rate (317 µmoL g$^{-1}$ h$^{-1}$) and O$_2$ evolution rate (168 µmol g$^{-1}$ h$^{-1}$) in 0.5 mM Co(bpy)$_3^{2+/3+}$ solution under visible light irradiation.

**Keywords:** Rh-doped SrTiO$_3$; hydrogen generation; Z-scheme overall water splitting

## 1. Introduction

Hydrogen is an environmentally clean chemical fuel with high energy density. Developing a photocatalyst system to generate hydrogen from water gives us a chance to produce hydrogen from an inexhaustible renewable source, i.e., sunlight and water. Much effort has been devoted to studies of the splitting of water into hydrogen and oxygen in the years following the discovery of photocatalytic water splitting using a semiconductor photoelectrode, TiO$_2$, as was demonstrated by Fujishima and Honda in 1972 [1]. From the thermodynamic perspective, it requires 237 kJ to transform one mole of water into hydrogen which is an energetically unfavorable uphill reaction. For a semiconductor photocatalyst for photocatalytic water-splitting reaction, the conduction band edge of the photocatalyst should be more negative than the reduction potential of H$_2$O to form H$_2$, and band edge of valence band should be more positive than the oxidation potential of H$_2$O is required to form O$_2$. The band gap of the semiconductor photocatalyst must be larger than the theoretical dissociation energy of the water molecule (1.23 eV). Several studies have reported that transition metal oxides with d$^0$ and d$^{10}$ electron configurations have showed photocatalytic activity of water splitting under UV light such as NaTaO$_3$ [2], K$_4$Nb$_6$O$_{17}$ [3] and M$_2$Sb$_2$O$_7$ (M = Ca, Sr) [4]. Since 1998, there have been several excellent reviews in photocatalysis water splitting [5–7]. The sun is the most important light source of our world. At sea level, there is only about 8% of solar ultraviolet radiation (200–400 nm), about 50% is

visible light, and about 40% is infrared radiation. Hence, numerous studies have attempted to develop highly efficient photocatalysts for water-splitting reaction which can be activated under visible light irradiation [8–10]. This improved photocatalytic activity can be achieved by introducing impurities such as transition metal [11] and non-metal elements [12] for a smaller band gap by lowering condition band edge or a rising valence band edge for use of solar light. However, a more negative conduction bend potential and a more positive valance band potential are thermodynamically favorable for the photocatalysis reduction and oxidation reactions. It is clear that satisfying these two conflicting conditions is a challenge for the development of visible light-responsive photocatalysts.

In recent years, a semiconductor-based Z-scheme system for overall water splitting has drawn much attention [13–15]. In a Z-scheme system, photocatalytic $H_2$ evolution and $O_2$ evolution occurs on two different photocatalysts and a redox couple as electron mediator. As compared to a conventional photocatalytic system with one photocatalyst, a Z-scheme system combines two photocatalysts for water reduction and oxidation where the electronic structure of the photocatalysts only have to satisfy the thermodynamics requirements to the half reactions for reduction and oxidation and thereby expands the variety of potential candidates for overall photocatalytic water splitting under visible light irradiation. In particular, $SrTiO_3$ photocatalyst has high potential for photocatalytic applications due to its high photocatalytic activity for water-splitting reaction. However, due to the wide band gap of $SrTiO_3$ (3.2 eV), intensive research has been carried out on doping transition metal ions in $SrTiO_3$ to reduce band gap and improve photocatalytic activity under visible light irradiation [16,17]. A visible-light-driven Z-scheme overall water-splitting system using Ru loaded Rh-doped $SrTiO_3$ (Ru/$SrTiO_3$:Rh) photocatalyst for $H_2$ evolution, $BiVO_4$ photocatalyst for $O_2$ evolution photocatalyst and a Tris (2,2′-bipyridine) cobalt(II)/Tris (2,2′-bipyridine) cobalt(III) used as electron mediator was achieved by Kudo and co-workers [13].

It is well known that, crystallinity is an important factor to influence photocatalytic activity. To achieve high crystalline quality, solid-state reaction is widely employed to synthesize semiconductor photocatalyst. However, the high-temperature synthesis process yields large particles and low surface area which is another important factor to consider. Several routes were taken to prepare $SrTiO_3$ nano particles via wet chemical route, including sol-gel synthesis and hydrothermal synthesis. It was reported that a variety of $SrTiO_3$ nanoparticles with specific morphologies such as nanocubes, nanowires, and porous structure can be fabricated via hydrothermal method [18].

In this paper, we present the synthesis of Rh-doped $SrTiO_3$ photocatalysts via a one-step microwave-assisted hydrothermal method. In the microwave-assisted hydrothermal process, heat was not only transferred from the outside to the inside of autoclave reactor as conventional heating, but also generated from the inside of $SrTiO_3$ due to its dielectric properties which led to a faster, and more efficient synthesis process [19]. By using anatase $TiO_2$ and $TiCl_4$ as titanium precursor, high crystallinity Rh-doped $SrTiO_3$ photocatalysts with different morphologies were synthesized quickly and efficiently, and no post treatment at high temperature was required. The influence of Ti precursors on the morphology of Rh-doped $SrTiO_3$ photocatalysts, as well as the photocatalytic activity for the Z-scheme overall water-splitting reaction under visible light irradiation were investigated. The results were compared with Rh-doped $SrTiO_3$ prepared by solid-state method and conventional hydrothermal method.

## 2. Materials and Methods

### 2.1. Synthesis of Rh-Doped SrTiO₃ with Ru Cocatalyst for H₂ Evolution

Two different titanium precursors, anatase $TiO_2$ (Alfa aesar) and $TiCl_4$ Alfa aesar), were used in the microwave-assisted hydrothermal synthesis of Rh-doped $SrTiO_3$.

The Rh-doped $SrTiO_3$ prepared by anatase $TiO_2$, MW-STO2Rh-A, were synthesized by using anatase $TiO_2$, $Sr(OH)_2$ and $Na_3RhCl_6$ as starting materials, where the molar composition of Ti:Sr:Rh was 100:98:2. The starting materials was added to 30 mL of 5M NaOH aqueous solution in sequence

under vigorous stirring. Then, the start material was transferred to a 100 cm$^3$ Teflon autoclave and the microwave-assisted hydrothermal treatment was performed in a commercial microwave digestion system (StartD, Milestone, Taiwan, 2011). The microwave hydrothermal process was performed at 180 °C for 1 h. After synthesis reactions, the product was washed by distillated H$_2$O and dried at 60 °C overnight.

The Rh-doped SrTiO$_3$ prepared by TiCl$_4$, referred as MW-STO2Rh-T, were synthesized by a similar procedure: TiCl$_4$, 1 M solution in toluene (Sigma-Aldrich, used as purchased), Sr(OH)$_2$ and Na$_3$RhCl$_6$ were used as starting materials where the molar composition of Ti:Sr:Rh was 100:98:2. The color of MW-STO2Rh-A and MW-STO2Rh-T varies from light yellow-green to gray-green. The color of samples became darker with increasing Rh amount.

In this study, conventional hydrothermal synthesis and solid-state synthesis of Rh-doped SrTiO$_3$ photocatalyst, denoted as HT-STO2Rh, and SS-STO2Rh were also prepared by for comparison. The HT-STO2Rh were synthesized by using anatase TiO$_2$, Sr(OH)$_2$ and Na$_3$RhCl$_6$ where the molar ratio of Ti:Sr:Rh= 100:98:2. The starting materials was added to 30 mL of 5M NaOH aqueous solution in sequence under vigorous stirring. The precursor solution was transferred to a 100 cm$^3$ Teflon lined autoclave. Then, the hydrothermal synthesis was carried out at 180 °C for 24 h. The HT-STO2Rh showed a similar color to that of MW-STO2Rh-A and MW-STO2Rh-T.

The SS-STO2Rh were prepared a two-step solid-state reaction using anatase TiO$_2$, SrCO$_3$, Rh$_2$O$_3$ (molar ratio 100: 98: 1). The mixed precursor was calcinated in air at 1273 K for 10h then at 1273 K for 10 h with an intermediate grinding process between the two calcinations; essentially similar of the procedure by Konta et al. [20]. The color of SS-STO2Rh was black.

Ru nanoparticles were used as a H$_2$ evolution cocatalyst and were loaded on Rh-doped SrTiO$_3$ by photo-deposition method. Rh-doped SrTiO$_3$ and an aqueous solution RuCl$_3$·xH$_2$O (1 wt % Ru loading for complete photoreduction) were added to a methanol solution (vol. ratio of MeOH:H$_2$O = 1:10). The suspension was irradiated in a photoreactor with a 400 W medium-pressure metal halide lamp (Phillips HPA400) for 12 h under string at room temperature. The sample was then filtered and washed with distilled water. Finally, the photocatalyst was dried at 60 °C overnight.

## 2.2. Synthesis of BiVO$_4$ for O$_2$ Evolution

The BiVO$_4$ photocatalyst for O$_2$ evolution was synthesized by microwave-assisted hydrothermal method. Bi$_2$O$_3$ and V$_2$O$_5$ in a molar ratio of 1:1 was added to 30 mL of 0.5 M HNO$_3$ solution under vigorous stirring for 20 min. Then, the starting materials was transferred to a 100 cm$^3$ Teflon reaction vessel and the microwave hydrothermal process was performed at 180 °C for 1 h. After synthesis reactions, the product was washed by distilled H$_2$O and dried at 60 °C overnight. The BiVO$_4$ photocatalyst had a vivid orange-yellow color.

## 2.3. Synthesis of [Co(bpy)$_3$]SO$_4$ for Electron Mediator

[Co(bpy)$_3$]SO$_4$ was synthesized by mixing stoichiometric amounts of CoSO$_4$·7H$_2$O and 2,2′-bipyridine (Bpy) in aqueous ethanol solution (vol. ratio of EtOH:H$_2$O = 2:1). The solution was heated under stirring to the ligand was totally dissolved. The mixture was cooled to room temperature, to precipitate the crude product. Then, the product was recrystallized to remove impurities [13].

## 2.4. Characterization and Photocatalytic Reactions

The characterization methods included Powder X-ray diffraction (XRD, Rigaku X-ray diffractometer, MAX-2500V, Cu-K$\alpha$ radiation, λ= 1.54178 Å), UV-vis diffuse reflectance spectra (Varian Lary 5E diode array spectrometer, Varian), and FE-SEM (Field emission scanning electron microscope, JSM-7000F, JEOL), and transmission electron microscopy (TEM, JEM-2000FX microscope, JEOL).

The photocatalytic reaction was carried out in a reactor equipped with an inner irradiation quartz cell with a cooling water jacket under stirring at 43 °C. A 150 W Xe lamp was mounted inside the quartz cell as shown in Figure 1. The photocatalytic Z-scheme water splitting was performed in

550 mL 0.5 mM aqueous Co(bpy)$_3$SO$_4$ solution containing 0.2 g of H$_2$ evolution and O$_2$ evolution photocatalysts, respectively. The photocatalysts were used as prepared without treatment. The gas product was analyzed by a gas chromatography (China Gas Chromatography 9800) with a packed column (MS-5A, 3.5 m in length) and thermal conductivity detector.
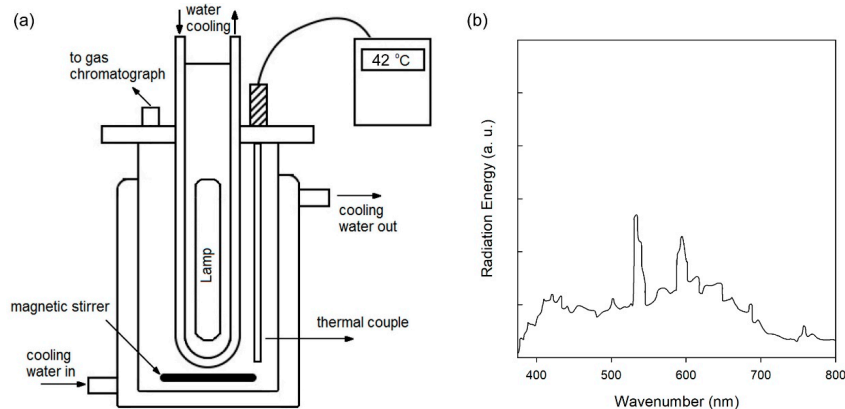


**Figure 1.** (**a**) Closed reaction system for photocatalysis water splitting (**b**) Emission spectrum of 150 W Xe lamp.

## 3. Results and Discussion

### 3.1. Characterization of the Hydrogen Evolution Catalyst: Rh-Doped SrTiO$_3$

Figure 2 shows the XRD patterns Rh-doped SrTiO$_3$ photocatalysts prepared by different methods: conventional solid-state reaction (SS), hydrothermal synthesis (HT) and microwave-assisted hydrothermal method (MW). The XRD patterns of all prepared materials show obvious diffraction peaks at $2\theta = 32.4°$, $40.0°$, $46.5°$, and $57.8°$ which corresponded to the (110), (111), (200) and (221) planes of SrTiO$_3$ (JCPDS 35-0734). No reflection peak corresponded to rhodium or rhodium oxide species of doping elements suggesting that dopant ions were introduced into structure of SrTiO$_3$ or were too small to be detected by XRD.
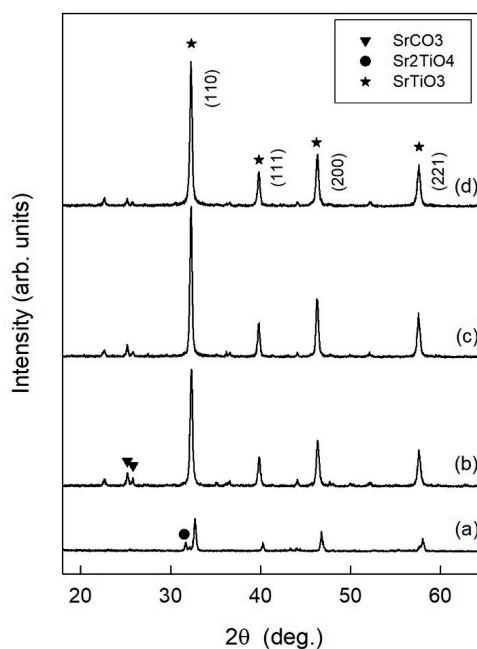


**Figure 2.** XRD patterns of Rh-doped SrTiO$_3$ catalysts (**a**) SS-STO2Rh (**b**) HT-STO2Rh (**c**) MW-STO2Rh-A (**d**) MW-STO2Rh-T.

The SS-STO2Rh showed a much weaker diffraction peaks than samples prepared via hydrothermal route. As compared with conventional solid-state reaction method, a better crystalline structure could be formed for Rh-doped SrTiO$_3$ prepared by hydrothermal synthesis. The small diffraction peaks at 2$\theta$ of 31.5° were considered as the presence of Sr$_2$TiO$_4$ (JCPDS-39-1471).

On the other hand, the XRD results also shows that samples prepared via hydrothermal route contained trace amount of SrCO$_3$ (JCPDS 84-0418, diffraction peaks located in 2$\theta$ of 20.5° and 25.4° as the (110) and (111) planes SrCO$_3$) for which was due to the reaction of environment CO$_2$ with the precursors such as Sr(OH)$_2$ and NaOH. The sharp diffraction peaks indicated that the samples were fully crystallized SrTiO$_3$ with cubic space group Pm3m (221). The average crystallite sizes of Rh-doped SrTiO$_3$ samples (HT-STO2Rh, MW-STO2Rh-A and MW-STO2Rh-T) prepared by hydrothermal method were about 3.6 nm, determined by Scherrer equation. It should be noted that while conventional hydrothermal synthesis of Rh-doped SrTiO$_3$ required a long synthesis time (>12 h), high crystallinity Rh-doped SrTiO$_3$ was formed in a very short time (about 1 h) during microwave-assisted hydrothermal synthesis [21]. These results indicated that the lattice deformation of Rh-doped SrTiO$_3$ are associated with the synthesis route.

To obtain the effects of synthesis route on their size and morphology, the samples were subjected to TEM analysis. Figure 3 depicts the TEM images of the Rh-doped SrTiO$_3$ prepared from different methods. The TEM results show that their morphology was significant different. The high-temperature solid-state synthesis caused the formation of large SS-STO2Rh particles with a diameter of 1–5 μm while the HT-STO2Rh catalyst showed smaller particles ranged from 50–500 nm. The TEM images also revealed that the MW-STO2Rh-A and MW-STO2Rh-T samples prepared by microwave-assisted hydrothermal method have a smallest particle sizes of about 100–200 nm. The TEM images also illustrated that the morphology Rh-doped SrTiO$_3$ by microwave-assisted hydrothermal method was changed sensitively by the titanium precursor. The MW-STO2Rh-A showed uniform cubic nano particles whereas the MW-STO2Rh-T showed a porous nanocrystal structure.
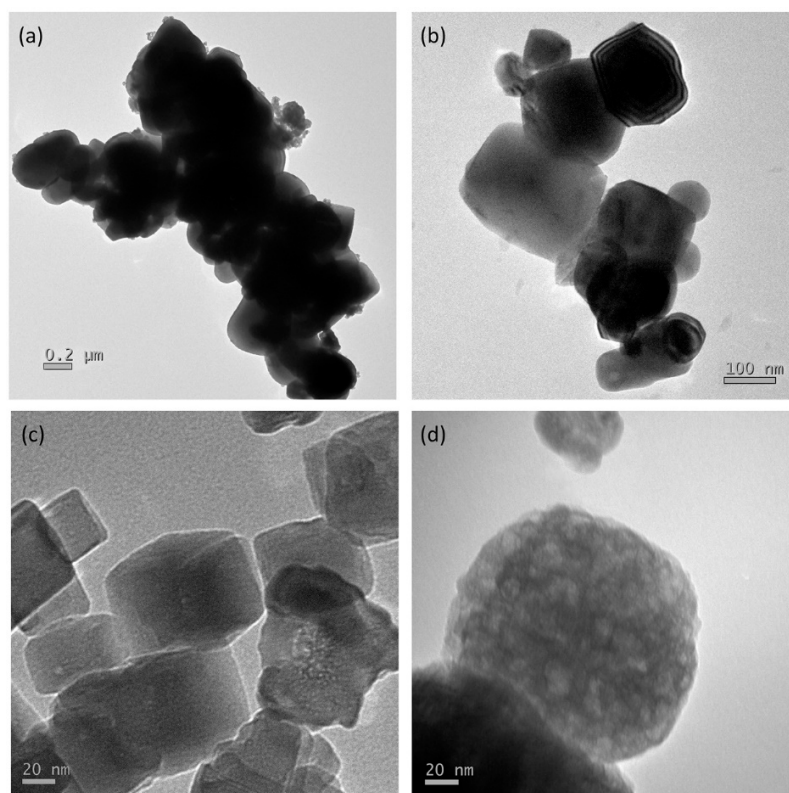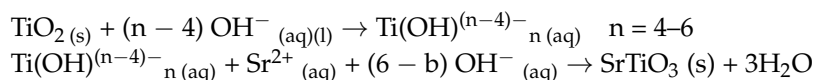


**Figure 3.** TEM images of Rh-doped SrTiO$_3$ catalysts (**a**) SS-STO2Rh (**b**) HT-STO2Rh (**c**) MW-STO2Rh-A (**d**) MW-STO2Rh-T.

Synthesis of anatase $SrTiO_3$ through hydrothermal reaction in NaOH solution was based on a series of dissolution-precipitation steps. The possible growth mechanism of $SrTiO_3$ nanoparticles form can be considered as following [18]:

$$TiO_{2\ (s)} + (n-4)\ OH^-_{\ (aq)(l)} \rightarrow Ti(OH)^{(n-4)-}_{\ n\ (aq)} \quad n = 4\text{–}6$$
$$Ti(OH)^{(n-4)-}_{\ n\ (aq)} + Sr^{2+}_{\ (aq)} + (6-b)\ OH^-_{\ (aq)} \rightarrow SrTiO_3\ (s) + 3H_2O$$

The $TiO_2$ can be dissolved in alkaline solution and converted to soluble $Ti(OH)^{(n-4)-}_n$, n = 4–6, and further form $SrTiO_3$ precipitation with $Sr^{2+}$ ion. Kalyani et al. [18] reported that the hydrothermal process of was limited by the dissolution rate of titanium precursor where cubic shape $SrTiO_3$ particles was formed form anatase $TiO_2$ precursor and porous $SrTiO_3$ particles was formed by $TiOCl_2$ due to its rapid hydrolysis of soluble titanium complexes at 200 °C for 13–24 h. In this study, we showed a porous nanosphere of Rh-doped $SrTiO_3$ can be synthesized by 1 M $TiCl_4$ in toluene as titanium precursor, where the rapid hydrolysis of $TiCl_4$ formed $Ti(OH)_n$ nano aggregates with a porous nanostructure in alkaline solution, which can be described as:

$$TiCl_{4\ (aq)} + 10\ H_2O \rightarrow Ti(OH)^-_5 + 5H_3O^+ + 4Cl^-$$
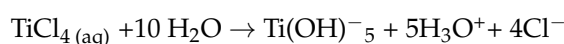
And reacted with $Sr^{2+}$ ions and form porous $SrTiO_3$ particles. Moreira et al. reported that the $TiCl_4$ formed $Ti(OH)^-_5$ and $Sr(OH)_2$ clusters, then strong and stable Ti-O-Ti and Sr-O-Sr bond was formed during the dehydration processes and self-assembled to form porous $SrTiO_3$ nanoparticles [22].

On the other hand, while small irregular particles (about 10–100 nm) was found in TEM image of SS-STO2Rh which could be $Rh_2O_3$ form via high-temperature solid-state reaction, no particles can be observed on the particle surfaces of HT-STO2Rh, MW-STO2Rh-A and MW-STO2Rh-T samples. It suggests that the Rh3+ ions from Na3RhCl6 were substituted into the Sr site of $SrTiO_3$ efficiently through liquid phase hydrothermal synthesis without forming of Rh or RhOx nanoparticles on the surface of $SrTiO_3$.

These results also indicated that while conventional hydrothermal synthesis of $SrTiO_3$ required a long synthesis time (>12 h), high crystallinity Rh-doped $SrTiO_3$ was formed in a very short time (about 1 h) during microwave-assisted hydrothermal synthesis.

Figure 4 shows the TEM images of Ru/MW-STO2Rh-A and Ru/MW-STO2Rh-T. As shown in Figure 4a, large Ru nanoparticles (>20 nm) were observed on the surface of MW-STO2Rh-A cubic nanoparticle. This suggests that Ru species could migrate easily along the particle surface of MW-STO2Rh-A, and form large Ru nanoparticles. On the other hand, the TEM image of Ru/MW-STO2Rh-T catalyst (Figure 4b) revealed clearly that about 2–5 nm Ru nanoparticles were formed on the rough particle surface of MW-STO2Rh-T. Our results showed that the deposition of Ru nanoparticles on the Rh-doped $SrTiO_3$ was affected by the surface morphology. The diffusion barrier of Rh species on a rough and porous surface was higher than on a well-crystallized $SrTiO_3$ particle with smooth surface. The precursor not only plays a significant role on particle morphology of Rh-doped $SrTiO_3$ photocatalysts but also the particle size distribution of Ru cocatalysts which were deposited to the surface of $SrTiO_3$ by photoreduction reaction.

The light absorption capacity of photocatalysts influences the efficiency of any photocatalytic reaction. Figure 5 shows the UV-vis diffuse reflectance spectra of the $SrTiO_3$ and Rh-doped $SrTiO_3$ samples prepared by different method. The band gap of the pristine $SrTiO_3$ (MW-STO-A) estimated form the absorption edge of the UV-vis spectrum was about 3.2 eV. As can be seen, the absorption edge of Rh-doped $SrTiO_3$ samples were clearly shifted to long wave region (Figure 5b–e). In this study, all the metal loading of catalysts was maintained at about 2 mol% to investigate the effects of other variables. Two shoulder peaks at 580 nm and 420 nm were observed in UV-vis spectra of Rh-doped $SrTiO_3$ samples which were attributed to the electron transition of the in-gap levels induced by Rh doping, corresponding to the existence of $Rh^{4+}$ and $Rh^{3+}$ species, respectively. As compared to SS-STO2Rh, and HT-STO2Rh prepared by conventional method, the MW-STO2Rh-A and MW-STO2Rh-T showed a lower absorption peak at 580 nm which suggested that the Rh-doped

$SrTiO_3$ prepared by microwave-assisted hydrothermal method consisted less $Rh^{4+}$ species than SS-STO2Rh prepared by solid-state method [23]. These results indicated donor and acceptor levels were introduced in the band gap of $SrTiO_3$ by the doping Rh.
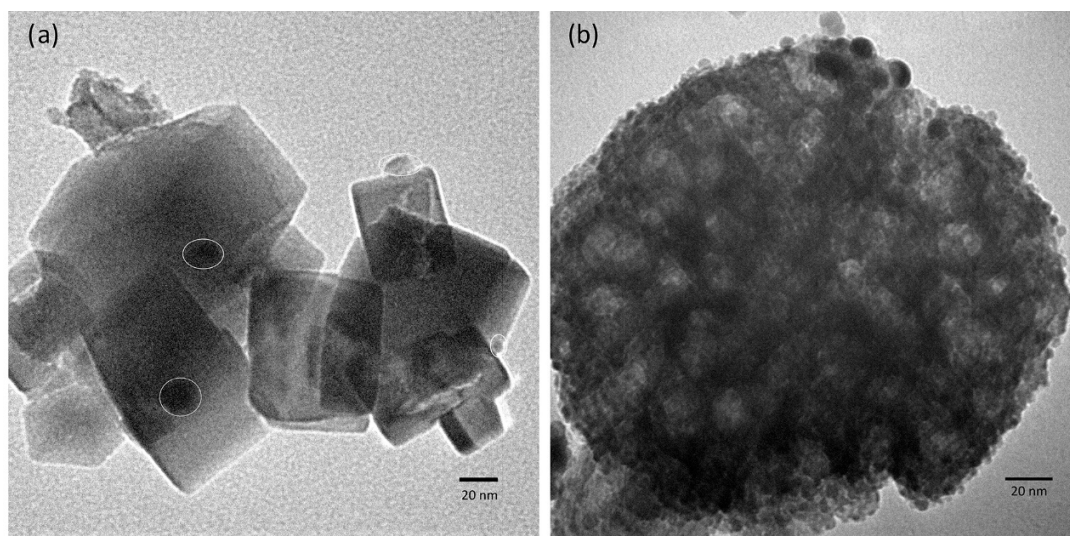


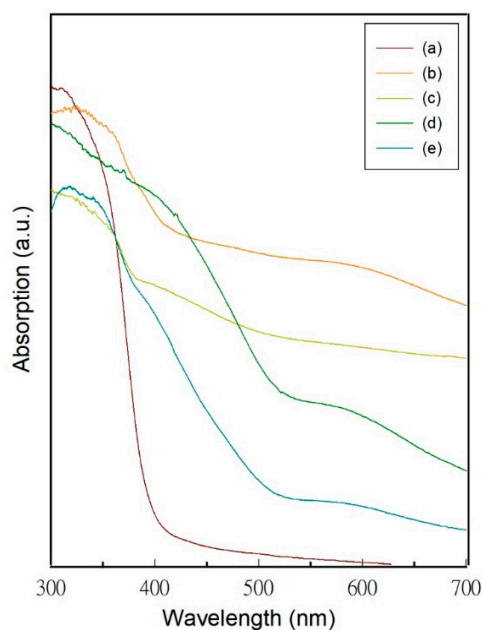**Figure 4.** TEM images of Rh-doped $SrTiO_3$ catalysts with Ru cocatalysts (**a**) Ru/MW-STO2Rh-A (**b**) Ru/MW-STO2Rh-T.



**Figure 5.** UV-vis spectra of Rh-doped $SrTiO_3$ catalysts (**a**) MW-STO-A (**b**) SS-STO2Rh (**c**) HT-STO2Rh (**d**) MW-STO2Rh-A (**e**) MW-STO2Rh-T.

*3.2. Characterization of the Oxygen Evolution Catalyst: BiVO4*

The XRD (Figure 6) results show that single phase monoclinic $BiVO_4$ (JCPDS 14-0688) was synthesized successfully by the microwave-assisted hydrothermal method. The optical absorption spectra of the $BiVO_4$ are shown in Figure 7. The strong absorption lies in visible light region from 400 nm to 550 nm. The band gap of the $BiVO_4$ sample estimated form the UV-vis spectrum was about 2.4 eV. Figure 8 depicts the SEM images of the $BiVO_4$ catalyst which are dual-faceted microcrystals with {010} and {110} facets [24].
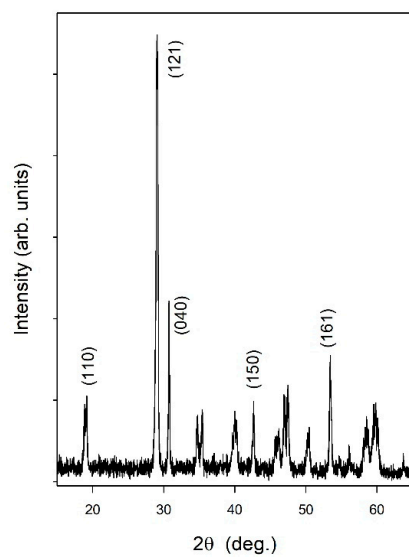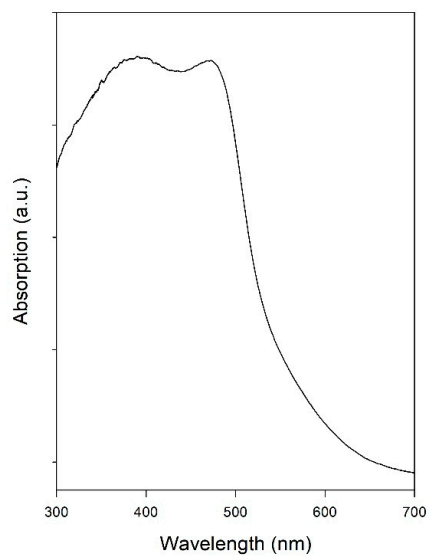
**Figure 6.** XRD spectrum of BiVO$_4$.
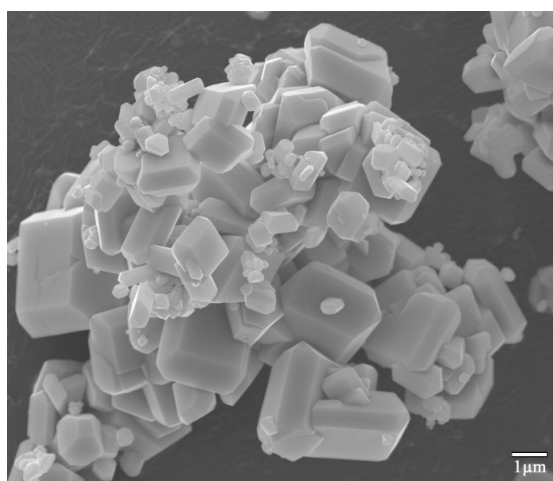


**Figure 7.** UV-vis spectrum of BiVO$_4$.



**Figure 8.** FE-SEM image of BiVO$_4$.

### 3.3. Photocatalytic Water-Splitting Activity

Figure 9 shows the $H_2$ and $O_2$ evolution time course on Ru/Rh:SrTiO$_3$–BiVO$_4$ photocatalysts taken from the 0.5 mM Co(bpy)$_3^{2+}$ solution. The gas production stopped when the light was turned off and similar hydrogen and oxygen production rates were observed in 8 h. This indicates that the Z-scheme overall water splitting on these catalysts was photocatalytic and that the photocatalysts can be used without deactivation. Furthermore, the $H_2$ and $O_2$ ratio of products were constant during the reaction and close to the theoretical stoichiometric ratio ($H_2/O_2 = 2$).
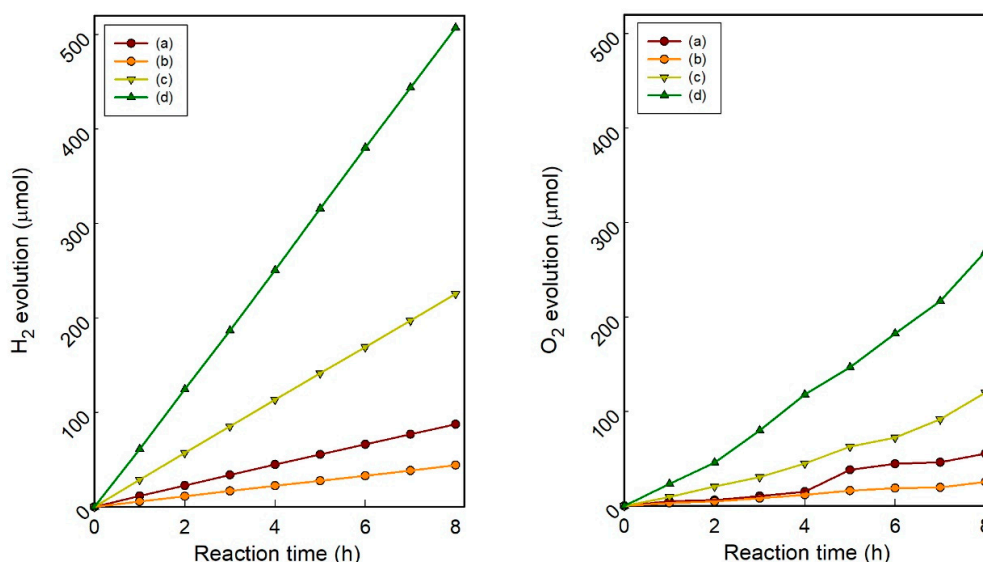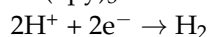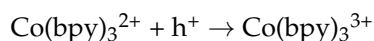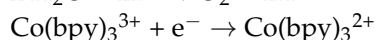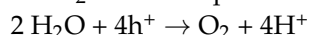


**Figure 9.** Time course of $H_2$ evolution and $O_2$ evolution for the Z-scheme photocatalysis water splitting on 1 wt % Ru/Rh:SrTiO$_3$–BiVO$_4$ where (**a**) Ru/SS-STO2Rh (**b**) Ru/HT-STO2Rh (**c**) Ru/MW-STO2Rh-A (**d**) Ru/MW-STO2Rh-T was used as $H_2$ evolution catalyst.

The related reactions of the Z-scheme photocatalytic water splitting are written as following [13]:
On $H_2$ evolution photocatalyst:

Co(bpy)$_3^{2+}$ + h$^+$ → Co(bpy)$_3^{3+}$
2H$^+$ + 2e$^-$ → $H_2$
On $H_2$ evolution photocatalyst:
2 H$_2$O + 4h$^+$ → $O_2$ + 4H$^+$
Co(bpy)$_3^{3+}$ + e$^-$ → Co(bpy)$_3^{2+}$

The average production rates of hydrogen and oxygen from water splitting over this period are listed in Table 1 which increased as the following order: Ru/HT-STO2Rh < Ru/SS-STO2Rh << Ru/MW-STO2Rh-A < Ru/SS-STO2Rh-T. These results show that the Rh-doped SrTiO$_3$ photocatalyst prepared by microwave-assisted hydrothermal method exhibited a very high hydrogen evolution rate of water-splitting reaction under visible light irradiation. The activity of Ru/SS-STO2Rh-T drastically increased more than 5 times as compared to Ru/SS-STO$_2$Rh, and 10 times than Ru/HT-STO prepared by convention hydrothermal method.

**Table 1.** Photocatalytic water-splitting activity of Rh-doped SrTiO$_3$–BiVO$_4$ in 0.5 mM CoBpy$^{2+/3+}$ solution.

| Catalyst | $H_2$ Evolution Rate (µmol eg$^{-1}$ h$^{-1}$) | $O_2$ Evolution Rate (µmol eg$^{-1}$ h$^{-1}$) |
|----------|-----------|-----------|
| Ru/SS-STO2Rh | 56 | 35 |
| Ru/HT-STO2Rh | 28 | 16 |
| Ru/MW-STO2Rh-A | 141 | 75 |
| Ru/MW-STO2Rh-T | 317 | 168 |

Conventional solid-state reaction is widely used to synthesize semiconductor photocatalyst. However, the high-temperature synthesis process leads to large particles and low surface area. It is known that preparation of photocatalyst nanoparticles via hydrothermal method. However, crystallinity is one of the most important factors of the photocatalytic activity of photocatalyst. Although HT-STO2Rh sample consisted smaller particles than SSR-STO2Rh sample, it showed a lower activity as compared to the SSR-STO2Rh sample.

Kato et al. [16] reported that the SrO defects in the Rh-doped $SrTiO_3$ photocatalyst prepared by hydrothermal method are the recombination centers for the photogenerated electron and holes which is the main reason of low activity. Their results indicated that a post calcination at 1273 K with excess Sr was necessary to decrease SrO defects of in the Rh-doped $SrTiO_3$ photocatalyst prepared by hydrothermal method. The low activity of Ru/HT-STO2Rh was attributed to the SrO defects formed in hydrothermal reaction.

The high activity of Ru/MW-STO2Rh-A and Ru/SS-STO2Rh-T samples indicated that the microwave-assisted hydrothermal method has distinct advantages in the synthesis of high crystallinity Rh-doped $SrTiO_3$ nanoparticles with low SrO defects. Secondly, a lower $Rh^{4+}$ cations as compared to that of $Rh:SrTiO_3$ prepared by conventional solid-state reaction and hydrothermal method may also play a role in improving activity of Ru/MW-STO2Rh-A and Ru/SS-STO2Rh-T samples [11]. Furthermore, the Ru/SS-STO2Rh-T showed a much higher activity than Ru/SS-STO2Rh-A. This suggests that the photo-excited electron can transfer more efficiently from SS-STO2Rh-T to the well dispersed Ru cocatalysts and reduce electron-hole recombination. On the other hand, the larger and less uniform Ru particles are attributed to the lower activity of Ru/MW-STO2Rh-A (Figure 4). Our results also show that the photocatalytic steps on $Ru/Rh:SrTiO_3$ is the rate limit step of the Z-scheme system of $Ru/Rh:SrTiO_3–BiVO_4$. The activity of $Ru/Rh:SrTiO_3$ is determined by complex factors, such as preparation method of $Rh:SrTiO_3$, titanium precursor, and the size and dispersion of Ru cocatalyst. It should be noticed that the photocatalysts were used as prepared without pretreatment. Therefore, it was believed that there were no effective heterojunctions between $Ru/Rh:SrTiO_3$ and $BiVO_4$ particles. The electron transformations were relied on $Co[(bpy)]_3^{2+/2+}$, the electron mediator redox couple. On the other hand, reduced graphene oxide as a solid electron mediator for Z-scheme water splitting was reported Iwase et al. [25] which indicated that the surface properties of the solid-state electron mediator played an important role for the photocatalytic activity. Our study has demonstrated a simple method to synthesize highly efficient photocatalysts by microwave-assisted hydrothermal method. Further studies are needed for the applications in a Z-scheme system with solid-state electron mediator.

## 4. Conclusions

In this study, we demonstrated that microwave-assisted hydrothermal method has distinct advantages in synthesis Rh-doped $SrTiO_3$ nanoparticles with high crystallinity. Our results showed that significant effect of Ti precursor on morphology of $Rh:SrTiO_3$. The $Rh:SrTiO_3$ nanoparticle in with uniform cubic structure and porous frameworks were successfully synthesized by anatase $TiO_2$ and $TiCl_4$ precursor, respectively. The $Rh:SrTiO_3$ prepared by the microwave-assisted hydrothermal method worked as a hydrogen evolution catalyst for the Z-scheme overall water-splitting system and exhibited a high and stable photocatalytic activities. The Ru/MW-STO2Rh-T-$BiVO_4$ Z-scheme system exhibited the highest photocatalytic activities with a rate $H_2$ evolution rate (317 $\mu mol\ g^{-1}\ h^{-1}$) and $O_2$ evolution rate (168 $\mu mol\ g^{-1}\ h^{-1}$) in 0.5 mM $Co(Bpy)_3^{2+/3+}$ solution under visible light irradiation. The great enhancement of photocatalytic activity of Ru/MW-STO2Rh is attributed to the levels enhanced visible light absorption by Rh donor levels and the efficient charge separation achieved by the highly dispersed Ru cocatalysts on the porous structure of MW-STO2Rh.

**Author Contributions:** All authors work together on performed the experiments and analysis data.

**Conflicts of Interest:** The authors declare no conflict of interest.

## References

1. Fujishima, A.; Honda, K. Electrochemical photolysis of water at a semiconductor electrode. *Nature* **1972**, *238*, 37–38. [CrossRef] [PubMed]
2. Kato, H.; Asakura, K.; Kudo, A. Highly Efficient water splitting into $H_2$ and $O_2$ over lanthanum-doped $NaTaO_3$ photocatalysts with high crystallinity and surface nanostructure. *J. Am. Chem. Soc.* **2003**, *125*, 3082–3089. [CrossRef] [PubMed]
3. Lin, H.Y.; Lee, T.H.; Sie, C.Y. Photocatalytic hydrogen production with nickel oxide intercalated $K_4Nb_6O_{17}$ under visible light irradiation. *Int. J. Hydrogen Energy* **2008**, *33*, 4055–4063. [CrossRef]
4. Sato, J.; Saito, N.; Nishiyama, H.; Inoue, Y. Photocatalytic water decomposition by $RuO_2$-loaded antimonates, $M_2Sb_2O_7$ (M = Ca, Sr), $CaSb_2O_6$ and $NaSbO_3$, with $d_{10}$ configuration. *J. Photochem. Photobiol. A* **2002**, *148*, 85. [CrossRef]
5. Takata, T.; Tanaka, A.; Hara, M.; Kondo, J.N.; Domen, K. Recent progress of photocatalysts for overall water splitting. *Catal. Today* **1998**, *44*, 17–26. [CrossRef]
6. Kudo, A.; Miseki, Y. Heterogeneous photocatalyst materials for water splitting. *Chem. Soc. Rev.* **2009**, *38*, 253–278. [CrossRef]
7. Li, X.; Yu, J.; Low, J.; Fang, Y.; Xiao, J.; Chen, X. Engineering heterogeneous semiconductors for solar water splitting. *J. Mater. Chem. A* **2015**, *3*, 2485–2534. [CrossRef]
8. Hisatomi, T.; Kubota, J.; Domen, K. Recent advances in semiconductors for photocatalytic and photoelectrochemical water splitting. *Chem. Soc. Rev.* **2014**, *43*, 7520–7535. [CrossRef]
9. Suzuki, T.M.; Iwase, A.; Tanaka, H.; Sato, S.; Kudo, A.; Morikawa, T. Z-scheme water splitting under visible light irradiation over powdered metal-complex/semiconductor hybrid photocatalysts mediated by reduced graphene oxide. *J. Mater. Chem. A* **2015**, *3*, 13283–13290. [CrossRef]
10. Lin, H.Y.; Shih, C.Y. Efficient one-pot microwave-assisted hydrothermal synthesis of M (M = Cr, Ni, Cu, Nb) and nitrogen co-doped $TiO_2$ for hydrogen production by photocatalytic water splitting. *J. Mol. Catal. A Chem.* **2016**, *411*, 128–137. [CrossRef]
11. Sasaki, Y.; Nemoto, H.; Saito, K.; Kudo, A. Solar Water Splitting Using Powdered Photocatalysts Driven by Z-Schematic Interparticle Electron Transfer without an Electron Mediator. *J. Phys. Chem. C* **2009**, *113*, 17536–17542. [CrossRef]
12. Asahi, R.; Morikawa, T.; Ohwaki, T.; Aoki, K.; Taga, Y. Visible-light photocatalysis in nitrogen-doped titanium oxides. *Science* **2001**, *293*, 269–271. [CrossRef] [PubMed]
13. Sasaki, Y.; Kato, H.; Kudo, A. $[Co(bpy)_3]^{3+/2+}$ and $[Co(phen)_3]^{3+/2+}$ Electron Mediators for Overall Water Splitting under Sunlight Irradiation Using Z-Scheme Photocatalyst System. *J. Am. Chem. Soc.* **2013**, *135*, 5441–5449. [CrossRef] [PubMed]
14. Maeda, K.; Lu, D.; Domen, K. Solar-Driven Z-scheme Water Splitting Using Modified $BaZrO_3$-BaTaO2N Solid Solutions as Photocatalysts. *ACS Catal.* **2013**, *3*, 1026–1033. [CrossRef]
15. Wang, Q.; Li, Y.; Hisatomi, T.; Nakabayashi, M.; Shibata, N.; Kubota, J.; Domen, K. Z-scheme water splitting using particulate semiconductors immobilized onto metal layers for efficient electron relay. *J. Catal.* **2015**, *328*, 308–315. [CrossRef]
16. Kato, H.; Sasaki, Y.; Shirakura, N.; Kudo, A. Synthesis of highly active rhodium-doped $SrTiO_3$ powders in Z-scheme systems for visible-light-driven photocatalytic overall water splitting. *J. Mater. Chem. A* **2013**, *1*, 12327–12333. [CrossRef]
17. Tonda, S.; Kumar, S.; Anjaneyulu, O.; Shanker, V. Synthesis of Cr and La-codoped $SrTiO_3$ nanoparticles for enhanced photocatalytic performance under sunlight irradiation. *Phys. Chem. Chem. Phys.* **2014**, *16*, 23819–23828. [CrossRef] [PubMed]
18. Kalyani, V.; Vasile, B.S.; Ianculescu, A.; Testino, A.; Carino, A.; Buscaglia, M.T.; Buscaglia, V.; Nanni, P. Hydrothermal Synthesis of $SrTiO_3$: Role of Interfaces. *Cryst. Growth Des.* **2015**, *15*, 5712–5725. [CrossRef]

19. Zheng, J.-Q.; Zhu, Y.-J.; Xu, J.-S.; Lu, B.-Q.; Qi, C.; Chen, F.; Wu, J. Microwave-assisted rapid synthesis and photocatalytic activity of mesoporous Nd-doped $SrTiO_3$ nanospheres and nanoplates. *Mater. Lett.* **2013**, *100*, 62–65. [CrossRef]

20. Konta, R.; Ishii, T.; Kato, H.; Kudo, A. Photocatalytic activities of noble metal ion doped $SrTiO_3$ under visible light irradiation. *J. Phys. Chem. B* **2004**, *108*, 8992–8995. [CrossRef]

21. Kiss, B.; Manning, T.D.; Hesp, D.; Didier, C.; Taylor, A.; Pickup, D.M.; Chadwick, A.V.; Allison, H.E.; Dhanak, V.R.; Claridge, J.B.; et al. Nano-structured rhodium doped $SrTiO_3$-Visible light activated photocatalyst for water decontamination. *Appl. Catal. B-Environ.* **2017**, *206*, 547–555. [CrossRef]

22. Moreira, M.L.; Longo, V.M.; Avansi, W., Jr.; Ferrer, M.M.; Andres, J.; Mastelaro, V.R.; Varela, J.A.; Longo, E. Quantum Mechanics Insight into the Microwave Nucleation of $SrTiO_3$ Nanospheres. *J. Phys. Chem. C* **2012**, *116*, 24792–24808. [CrossRef]

23. Kawasaki, S.; Akagi, K.; Nakatsuji, K.; Yamamoto, S.; Matsuda, I.; Harada, Y.; Yoshinobu, J.; Komori, F.; Takahashi, R.; Lippmaa, M.; et al. Elucidation of Rh-Induced In-Gap States of $Rh:SrTiO_3$ Visible-Light-Driven Photocatalyst by Soft X-ray Spectroscopy and First-Principles Calculations. *J. Phys. Chem. C* **2012**, *116*, 24445–24448. [CrossRef]

24. Tan, H.L.; Tahini, H.A.; Wen, X.; Wong, R.J.; Tan, X.; Iwase, A.; Kudo, A.; Amal, R.; Smith, S.C.; Ng, Y.H. Interfacing $BiVO_4$ with Reduced Graphene Oxide for Enhanced Photoactivity: A Tale of Facet Dependence of Electron Shuttling. *Small* **2016**, *12*, 5295–5302. [CrossRef] [PubMed]

25. Iwase, A.; Ng, Y.H.; Ishiguro, Y.; Kudo, A.; Amal, R. Reduced graphene oxide as a solid-state electron mediator in Z-scheme photocatalytic water splitting under visible light. *J. Am. Chem. Soc.* **2011**, *133*, 11054–11057. [CrossRef] [PubMed]